Revisiting $O(N)$ σ model at unphysical pion masses and high temperatures

Yuan-Lin Lyu,[1,‡] Qu-Zhi Li,[2,*] Zhiguang Xiao,[2,†] and Han-Qing Zheng[2,§]
[1]*School of Physics, Peking University, Beijing 100871, People's Republic of China*
[2]*Institute for Particle and Nuclear Physics, College of Physics, Sichuan University, Chengdu 610065, People's Republic of China*

(Received 12 March 2024; accepted 18 April 2024; published 13 May 2024)

Roy-equation analysis on lattice data of $\pi\pi$ scattering phase shifts at $m_\pi = 391$ MeV reveals that the lowest f_0 meson becomes a bound state under this condition. In addition, there is a pair of complex poles below threshold generated by crossing symmetry [X.-H. Cao *et al.*, Phys. Rev. D **108**, 034009 (2023)]. We use the N/D method to partially recover crossing symmetry of the $O(N)$ σ model amplitude at leading order of $1/N$ expansion, and qualitatively reproduce the pole structure and pole trajectories with varying pion masses as revealed by Roy-equation analyses. The σ pole trajectory with varying temperature is also discussed and found to be similar to its properties when varying m_π. As the temperature increases, the complex σ poles firstly move from the second Riemann sheet to the real axis becoming two virtual state poles, and then one virtual state pole moves to the first sheet turning into a bound state pole and finally tends to the pion pole position at high temperature which is as expected from the chiral symmetry restoration. Our results provide further evidence that the lowest f_0 state extracted from experiments and lattice data plays the role of the σ meson in the spontaneous breaking of chiral symmetry. Finally, we also briefly discuss the problems of the effective potential in the situation when m_π and the temperature become large.

DOI: 10.1103/PhysRevD.109.094026

I. INTRODUCTION

Chiral symmetry breaking plays an important role in the QCD low energy dynamics. It is already well known that due to the smallness of the u and d quark masses, QCD possesses an approximate $SU(2)_L \times SU(2)_R$ chiral symmetry, and it is also well accepted that this symmetry is spontaneously broken by the nonzero $\langle 0|\bar{q}q|0\rangle$ and three pseudo-Goldstone bosons are generated which are identified as the π mesons observed in the low energy hadron scatterings. Historically, the famous linear sigma model firstly proposed by Gell-Mann and Lévy in 1960 [1] could provide an effective field theory description of this symmetry. In this model, another scalar field σ is combined with the three pions to form a linear realization of an $O(4)$ symmetry and acquires a vacuum expectation value (VEV) to break the $O(4)$ to $O(3)$, where the $O(4) \simeq SU(2)_L \times SU(2)_R$ can be identified as the previous chiral symmetry and the remaining $O(3)$ corresponds to the preserved $SU(2)_V$. For a long time, the existence of the σ particle was in controversy. The mild rise of the $\pi\pi$ phase shift can hardly be recognized as generated from a typical resonance. A broad resonance was proposed to describe the $\pi\pi$ scattering phase shift in the 1960s, see for example [2–4]. However, such a broad resonance appeared and disappeared from the PDG table several times from the 1960s until the 2000s.

Another description using a nonlinear realization of the chiral symmetry [5,6] in which the scalar-isoscalar particle is totally abandoned from the Lagrangian is the nowadays very popular chiral perturbation theory (χPT) [7,8], which is regarded as the low energy effective theory of QCD. Within this formalism, the low energy properties of the pion-pion scattering, such as the scattering length, effective range, and phase shifts near the threshold can be reproduced. The low energy coupling constants can be saturated by integrating out vector resonances [9,10] (see however [11,12]). Thus, there seems to be no need to have a scalar-isoscalar particle in describing the low energy pion-pion scatterings. However, with energy going up, χPT blows up quickly. Fortunately, unitarity and dispersive techniques come to its rescue. After unitarization, the $IJ = 00$ channel $\pi\pi$ scattering amplitude dynamically generates a resonance state represented as a pair of conjugate poles on the second

*Corresponding author: liquzhi@scu.edu.cn
†Corresponding author: xiaozg@scu.edu.cn
‡yllyu@stu.pku.edu.cn
§zhenghq@pku.edu.cn

Riemann sheet, see for example [13,14]. However, this kind of unitarized method always generates more poles than physically expected [15], especially spurious poles on the physical sheet, which cast doubts on the reliability of the results, not to mention the violation of crossing symmetry (for a recent review, see Ref. [16]). On the other hand, a novel model-independent analysis representing the partial wave S-matrix as a product of pole and the left-hand cut integral terms showed that the left-hand cut estimated from χPT always produces a negative contribution to the phase shift while the data show a positive trend near the threshold, which demonstrates the necessity of a subthreshold resonance pole on the second sheet of the amplitude [17]. This method was further developed into the so-called Peking University (PKU)-representation of the partial wave S-matrix [18–22], and more precise mass and width for the particle was obtained by fitting the data with the constraints from Balachandran-Nuyts-Roskies (BNR) relations derived from crossing symmetry [19].

A major step forward in analyzing the pion-pion scattering data is the so-called Roy-equation analysis [23] which incorporates crossing symmetry and unitarity into a set of integral equations involving only the partial wave amplitudes in the physical region. By solving these integral equations with the low energy constraints from χPT [24,25] and extending the solution to the complex plane, a broad resonance pole can be found around $\sqrt{s_{\rm pole}} = 441^{16}_{-8} - i272^{+9}_{-13}$ MeV [26] (see also [27–29]). From these model-independent efforts, the existence of a scalar-isoscalar resonance in the low energy $\pi\pi$ scattering was firmly established, and up to now PDG lists the particle as $f_0(500)$ with a pole mass in 400–550 MeV and the half-width around 200–350 MeV.

Although these model-independent methods confirm the existence of this particle, it is obscure what the role of this scalar-isoscalar particle plays in the low energy QCD spectrum and chiral symmetry breaking. An argument showing that this $f_0(500)$ is not a usual pure $\bar{q}q$ state is that with large number of colors, N_c, the pole generated in the unitarized χPT goes away from the real axis which is different from the usual meson behavior in the large N_c limit [13]. However, for large enough N_c, the pole position still moves toward the real axis [30]. Another problem is whether it really corresponds to the original σ particle in the Lagrangian models with linearly realized chiral symmetry, which is still not clearly understood (see for example, Ref. [31]). Within the unitarized χPT framework, the $f_0(500)$ particle is only a dynamically generated resonance without any useful information about the role it plays in the chiral symmetry breaking. This can be understood since χPT starts off from the broken phase of QCD with a nonzero VEV, it may not provide much information about the global property of the effective potential which is responsible for symmetry breakdown. Moreover, a study of χPT at high temperatures reveals its drastic difference compared with the linear σ model: the former simply cannot restore the wanted $O(4)$ symmetry explicitly, though there are some implicit evidences [32–36]. So to analyze the role played by this particle, it is desirable to look back at the linear σ model to see whether the sigma particle in this model is consistent with $f_0(500)$ in model-independent analyses. One advantage of the $O(N)$ linear σ model is that in the large N limit (here N denotes the number of flavors), the model is exactly solvable [37–39] and has been used to study the possible relation between $f_0(500)$ and the σ [40].

With the recent development of lattice QCD [41–51], phase shifts of $\pi\pi$ scattering can be reproduced from the first principle at various unphysical pion masses. This provides additional valuable information for the resonances in $\pi\pi$ scattering by extracting pole positions from those phase shifts. In Ref. [49], the scattering phase shifts for the $IJ = 00$ channel are calculated at $m_\pi \sim 236$ and 391 MeV, and K-matrix parametrization was used to extract the poles in this channel. The result shows that when $m_\pi \sim 236$ MeV the lowest f_0 state is still a resonance while at 391 MeV it becomes a bound state.

More recent results by the HadSpec Collaboration using the similar K-matrix method shows that at $m_\pi \sim 330$ MeV, σ already becomes a shallow bound state, whereas at $m_\pi \sim 283$ MeV it may become a virtual state or a subthreshold resonance [51]. In fact, it has been suggested that in the unitarized χPT amplitudes with larger pion masses, the dynamically generated f_0 particle moves toward the real axis below threshold and finally becomes a bound state [52–54]. However, it is well known that the K-matrix approach does not satisfy crossing symmetry [11,12], which is important in the low energy pion-pion scattering and is crucial in determining the properties of $f_0(500)$ resonance [19,28,29]. The first attempt to incorporate crossing symmetry in the analysis is in Ref. [55], where the PKU representation combined with BNR relations and a virtual state accompanying the f_0 bound state was found at $m_\pi = 391$ MeV. However, it was noticed that the left-hand cut considered in that paper is not complete: the left-hand cut contribution introduced by the f_0 bound state from crossed channels was not taken into account [56].

Not only in Ref. [55], the situation in general is also unsatisfactory. Model-independent lattice data were always analyzed using rough models. A precise model-independent analysis of lattice data using Roy-equation analysis which incorporates crossing symmetry from the startup was done in Ref. [57]. It is also found that on the second sheet there is a pair of conjugate subthreshold poles generated, which is related to the left-hand cut originated from the f_0 bound state in crossed channels. A general argument of why this subthreshold pole is present was also given in Ref. [57]. Recently, a further lattice study using Roy-equation analysis at $m_\pi \sim 239$ and 283 MeV found that for the former, the lowest f_0 state remains a resonance, whereas in the latter

case the state was claimed (though not definitively, see Ref. [58] for details) to become a virtual state, accompanied by a "noisy" pole close to the left-hand cut on the second Riemann sheet. However, this additional virtual state pole is generated before the f_0 particle turns into a bound state, a situation not considered in Ref. [57]. To one's surprise, this phenomenon is exactly what happens in the N/D modified $O(N)$ model and we will explain the details in Sec. III.

The phenomena at unphysical pion masses provide a new test ground of whether the lowest f_0 state in model-independent analyses corresponds to the σ particle in the linear σ model. The purpose of this paper is to use the solvable $O(N)$ linear σ model with a crossing symmetry improvement at unphysical pion masses and compare it with the results from Roy-equation analyses.

The paper is organized as follows. In Sec. II, a review on standard results of the $O(N)$ model is given, especially the behavior of the lowest f_0 particle is discussed and compared with similar results obtained by different model analyses of the lattice data. The comparison necessitates the effort of going beyond the lowest order calculation of the $O(N)$ model. In Sec. III, the modified $O(N)$ amplitude incorporating crossing symmetry is introduced, aided by the use of N/D method. The results from Roy-equation analyses on the σ particle can be reproduced in this approach at a qualitative level. In particular, the f_0 state becomes a bound state and the lower subthreshold pole generated through cross-channel effects also emerges at $m_\pi = 391$ MeV after partially imposing crossing symmetry, by tuning the parameters in the N/D method. Though it is well known that the linear σ model is not QCD [7,8], this paper is trying to demonstrate that it provides a qualitative description of low energy QCD in the $IJ = 00$ channel at the phenomenological level, even for unphysical pion masses—from this observation we take the perspective that the $f_0(500)$ particle plays the role of the σ particle. In Sec. IV, we also investigate thermal properties of the scattering amplitudes with leading order $1/N$ expansion. We reproduce the widely accepted results that $O(N)$ symmetry is restored at high temperature, irrespective of different m_π values. Finally Sec. V is for discussions and conclusions, where we shortly discuss the problem that the effective potential no longer provides a local minimum at high temperature, as well as when m_π gets large. Future improvements on the related issues are also outlined there.

II. σ POLE WITH VARYING m_π IN $O(N)$ MODEL

In this section, we will review the $O(N)$ linear σ model and look at the σ pole trajectory with varying m_π, at leading order of $1/N$ expansion. The Lagrangian for this model is

$$\mathcal{L}_{O(N)} = \frac{1}{2}\partial_\mu\phi_a\partial^\mu\phi_a - \frac{1}{2}\mu_0^2\phi_a\phi_a - \frac{\lambda_0}{8N}(\phi_a\phi_a)^2 + \alpha\phi_N, \tag{1}$$

where $a = 1, 2, \ldots, N$. When $\mu_0^2 < 0$, without the linear α term, the system has a spontaneous symmetry breaking of $O(N) \to O(N-1)$, $\langle\phi\rangle \neq 0$. With the linear ϕ_N term, the VEV is aligned with the Nth direction, namely, $\langle\phi_N\rangle = v$, with $N-1$ pseudo-Goldstone particles, $\pi_a \equiv \phi_a$, $a = 1, \ldots, N-1$ and we define the shifted field $\sigma \equiv \phi_N - v$. For convenience when counting $1/N$ orders in the calculation of the effective action, we introduce an auxiliary field χ to the Lagrangian [39],

$$\begin{aligned}\mathcal{L} &\to \mathcal{L} + \frac{N}{2\lambda_0}\left(\chi - \frac{\lambda_0}{2N}\phi_a\phi_a - \mu_0^2\right)^2 \\ &= \frac{1}{2}\partial_\mu\phi_a\partial^\mu\phi_a + \alpha\phi_N + \frac{N}{2\lambda_0}\chi^2 - \frac{1}{2}\chi\phi_a\phi_a - \frac{N\mu_0^2}{\lambda_0}\chi,\end{aligned} \tag{2}$$

with an irrelevant constant omitted. The effective action can be obtained by standard procedures,

$$\begin{aligned}\Gamma(\phi,\chi) = \int \mathrm{d}^4x\Big(&\frac{1}{2}\partial_\mu\phi_a\partial^\mu\phi_a + \alpha\phi_N + \frac{N}{2\lambda_0}\chi^2 - \frac{1}{2}\chi\phi_a\phi_a \\ &- \frac{N\mu_0^2}{\lambda_0}\chi\Big) + \frac{i}{2}N\mathrm{Tr}\log(\partial^2 + \chi - i\epsilon),\end{aligned} \tag{3}$$

where Tr denotes trace taken in four-dimensional Minkowski spacetime and $\epsilon \to 0^+$. For convenience we will not distinguish the notation for the classical fields and the original fields in the Lagrangian, which can be understood in the context. Then the effective potential can be obtained as

$$\begin{aligned}V(\phi,\chi) = &-\alpha\phi_N - \frac{N}{2\lambda_0}\chi^2 + \frac{1}{2}\chi\phi_a\phi_a + \frac{N\mu_0^2}{\lambda_0}\chi \\ &- \frac{i}{2}N\int\frac{d^4\ell}{(2\pi)^4}\log(-\ell^2 + \chi - i\epsilon),\end{aligned} \tag{4}$$

where ϕ_a, χ are regarded as their constant expectation values, respectively. The renormalization conditions are chosen to be [39,59]

$$\frac{\mu(M)^2}{\lambda(M)} = \frac{\mu_0^2}{\lambda_0} + \frac{i}{2}\int\frac{d^4\ell}{(2\pi)^4}\frac{1}{\ell^2 + i\epsilon}, \tag{5}$$

$$\frac{1}{\lambda(M)} = \frac{1}{\lambda_0} - \frac{i}{2}\int\frac{d^4\ell}{(2\pi)^4}\frac{1}{(\ell^2 + i\epsilon)(\ell^2 - M^2 + i\epsilon)}. \tag{6}$$

With these conditions, the minimum of the effective potential can be obtained by solving $\frac{\partial V}{\partial\chi} = 0$ and $\frac{\partial V}{\partial\phi_a} = 0$ which reduce to relations of the VEVs for the corresponding fields

$$\phi_a\phi_a = \frac{2N}{\lambda}\chi - \frac{2N\mu^2}{\lambda} - \frac{N}{16\pi^2}\chi\log\frac{\chi}{M^2}, \tag{7}$$

$$\chi\phi_a = 0 (a < N), \qquad \chi\phi_N - \alpha = 0. \tag{8}$$

Thus, the VEV for each π_a is still zero, i.e. $\langle\pi_a\rangle = 0$ and ϕ_N gets expectation value $\langle\phi_N\rangle = v = \alpha/\langle\chi\rangle$. Since the correction to the pion mass term only appears at higher $1/N$ order, at leading order we have $\langle\chi\rangle = m_\pi^2$. At zero temperature, from the definition of the pion decay constant f_π, $\langle 0|A_a^\mu(x)|\pi\rangle = ip^\mu f_\pi e^{-ip\cdot x}$, where A_a^μ is the axial vector current, and the relation of partially conserved axial current (PCAC), $\partial_\mu A_a^\mu = \alpha\pi_a$, we have $v = f_\pi$. For phenomenological calculations, we always set $f_\pi = 92.4$ MeV and $N = 4$.

With these preparations, now the $\pi\pi$ scattering amplitude in the leading $1/N$ order can be expressed according to the external isospin structure as follows,

$$\mathcal{T}_{\pi_a\pi_b\to\pi_c\pi_d} = iD_{\tau\tau}(s)\delta_{ab}\delta_{cd} + iD_{\tau\tau}(t)\delta_{ac}\delta_{bd} + iD_{\tau\tau}(u)\delta_{ad}\delta_{bc}, \tag{9}$$

with $D_{\tau\tau}$ the propagator for $\tau \equiv \chi - \langle\chi\rangle$ field from the effective action. Since there are mixing terms of τ and σ, a 2×2 inverse propagator matrix needs to be considered [39,59], which can be expressed in the momentum space as

$$D^{-1}(p^2) = -i\begin{pmatrix} p^2 - m_\pi^2 & -f_\pi \\ -f_\pi & N/\lambda_0 + NB_0(p^2, m_\pi)\end{pmatrix}, \tag{10}$$

with

$$B_0(p^2, m_\pi) = \frac{-i}{2}\int\frac{d^4\ell}{(2\pi)^4}\frac{1}{(\ell^2 - m_\pi^2 + i\epsilon)((\ell+p)^2 - m_\pi^2 + i\epsilon)}. \tag{11}$$

The propagators can then be obtained as

$$D_{\tau\tau}(p^2) = \frac{i(p^2 - m_\pi^2)}{(p^2 - m_\pi^2)(N/\lambda_0 + NB_0(p^2, m_\pi)) - f_\pi^2}, \tag{12}$$

$$D_{\sigma\sigma}(p^2) = \frac{i(1/\lambda_0 + B_0(p^2, m_\pi))}{(p^2 - m_\pi^2)(1/\lambda_0 + B_0(p^2, m_\pi)) - f_\pi^2/N}. \tag{13}$$

Using the previous renormalization conditions Eqs. (5) and (6), we have

$$\frac{1}{\lambda_0} + B_0(p^2, m_\pi) = \frac{1}{\lambda(M)} + B(p^2, m_\pi, M), \tag{14}$$

$$B(s, m_\pi, M) = \frac{1}{32\pi^2}\left(1 + \rho(s)\log\frac{\rho(s) - 1}{\rho(s) + 1} - \log\frac{m_\pi^2}{M^2}\right), \tag{15}$$

where $\rho(s) = \sqrt{1 - 4m_\pi^2/s}$. For our purpose, we need only $IJ = 00$ amplitude in the leading order of $1/N$ expansion,

$$\mathcal{T}_{00}^{\mathrm{LO}}(s) = \frac{iND_{\tau\tau}(s)}{32\pi}, \tag{16}$$

which is of $\mathcal{O}(1)$.

The σ resonance corresponds to poles on the second Riemann sheet, which can be obtained by solving the zero points of the denominator of $D_{\tau\tau}$:

$$(s - m_\pi^2)(1/\lambda(M) + B^{II}(s, m_\pi, M)) - f_\pi^2/N = 0, \tag{17}$$

where B^{II} represents the analytically continued $B(s, m_\pi, M)$ function onto the second sheet, which is obtainable by changing the sign of $\rho(s)$.

Since the coupling constant λ and the renormalization scale M are related, we can define M to be the intrinsic scale of the $O(N)$ model, when regarded as an effective field theory, at which the coupling blows up, i.e. $1/\lambda(M) = 0$ [59]. Then the coupling λ would not appear in the scattering amplitude,

$$\mathcal{T}_{00}^{\mathrm{LO}}(s) = -\frac{1}{32\pi}\frac{s - m_\pi^2}{(s - m_\pi^2)B(s, m_\pi, M) - f_\pi^2/N}, \tag{18}$$

and Eq. (17) can be recast into

$$(s - m_\pi^2)B^{II}(s, m_\pi, M) - f_\pi^2/N = 0. \tag{19}$$

The leading order amplitude automatically satisfies the exact partial wave unitarity, i.e. $\mathrm{Im}\mathcal{T}_{00}(s) = \rho(s)|\mathcal{T}_{00}(s)|^2$. It also has an Adler zero [60] at $s = m_\pi^2$. Notice that the isospin projection for the $O(N)$ singlet channel is $\mathcal{T}_{I=0}(s,t,u) = (N-1)iD_{\tau\tau}(s) + iD_{\tau\tau}(t) + iD_{\tau\tau}(u)$. Thus the t- and u-channel amplitudes in Eq. (9) contribute to the $\mathcal{O}(1/N)$ amplitude, and only the s-channel amplitude contributes to the leading order $IJ = 00$ partial wave amplitude. This already breaks crossing symmetry.

With the leading order $\mathcal{T}$ matrix, we can study the σ pole trajectory with varying m_π. The intrinsic scale M is chosen at 550 MeV. See Table I for comparison of the pole positions obtained in the $O(N)$ model and the lattice results analyzed using K matrix and Roy equation respectively. The pole trajectory is shown in Fig. 1. When m_π increases from the physical mass, the σ poles move toward the real axis, and then become two virtual state poles (VS I and II) after they meet at the real axis. One virtual state pole (VS II) moves down away and the other (VS I) moves toward the threshold, crossing it to the first sheet, and becomes a bound state (BS) pole.

From Eq. (19) one can work out the condition for the critical pion mass $m_\pi = m_c$ at which the σ pole is located exactly at the threshold,

$$\log\frac{m_c^2}{M^2} = 1 - \frac{32\pi^2 f_\pi^2}{3m_c^2 N}. \tag{20}$$

TABLE I. Comparison of the pole positions ($\sqrt{s_{\rm pole}}$) for $O(N)$ model, lattice + K matrix [49,51] and lattice + Roy equation [57,58]. When $m_\pi = 391$ MeV, the subthreshold (Sub.) pole close to the left-hand cut in Ref. [57] can also be found (qualitatively) within the N/D modified $O(N)$ model discussed in this work.

m_π (MeV)	139	239	283	330	391
$O(N)$ (LO)	$356 - i148$	$448 - i57$	558(VS I) 438(VS II)	660(VS I) 451(VS II)	780(BS) 489(VS II)
N/D modified $O(N)$	$348 - i180$	469(BS) 426(VS II) 168(VS III)	527(BS) 422(VS II) 264(VS III)	585(BS) $396 - i28$ (Sub pole)	658(BS) $466 - i77$ (Sub pole)
lattice + K-matrix		(487–809 $-i$136–304) [49,51]	(476–579 $-i$0–129) [51]	657^{+3}_{-4}(BS) [51]	758 ± 4(BS) [49]
lattice + Roy equation		(416–644 $-i$176–307) [57,58]	522–562 (VS I&II) [58][a]		759^{+7}_{-16}(BS) [57] $269^{+40}_{-25} - i211^{+26}_{-23}$ (Sub pole) [57]

[a]Additionally, there is a third though "noisy" pole close to the left-hand cut on the second sheet, which could correspond to the virtual state pole VS III appearing in the N/D modified $O(N)$ model analysis. However, a definitive conclusion about whether the σ is a virtual state or a subthreshold resonance at this m_π value cannot be made, owing to large statistical uncertainties in the results, see Ref. [58] for details.

The numerical result is $m_c \simeq 337$ MeV. This is a little bit different from the lattice results which may be located at somewhere between 283 and 330 MeV [49,51,58]. The difference is not surprising since the m_c obtained here is only the leading $1/N$ order result of $O(N)$ model. When $m_\pi > m_c$, the σ particle becomes a bound state. At the same time, it also appears in the t- and u-channel amplitudes due to crossing symmetry, which are not included in the leading order amplitude since they are of $\mathcal{O}(1/N)$ after isospin projection. If we add the t- and u-channel contributions and do the isospin and partial wave projection, then the $\mathcal{T}_{00}$ matrix is expressed as

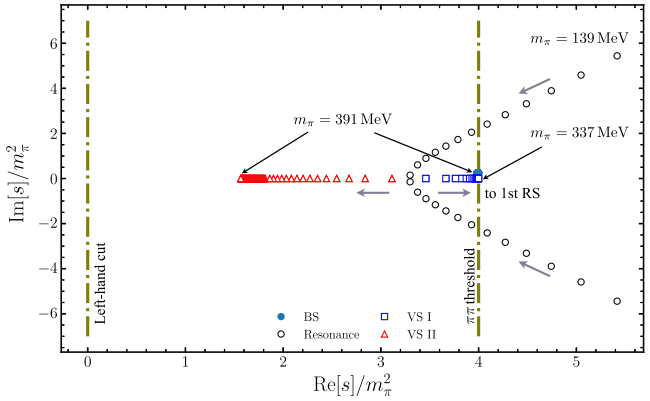

FIG. 1. Pole trajectories for the σ poles of the leading order $O(N)$ amplitude. The left-hand cut branch point is still at $s_L = 0$ after the virtual state pole VS I moves across threshold to the physical Riemann sheet (RS), becoming a bound state. There is neither an additional virtual state pole generated from the left-hand cut (suggested by Refs. [57,58]), nor subthreshold poles similar to those found in Ref. [57].

$$\mathcal{T}_{00}(s) = \frac{N-1}{32\pi}\mathcal{A}^{\rm LO}(s) + I_{tu}(s), \tag{21}$$

where

$$\mathcal{A}^{\rm LO}(s) = \frac{m_\pi^2 - s}{(s-m_\pi^2)NB(s,m_\pi,M) - f_\pi^2}, \tag{22}$$

$$I_{tu}(s) = \frac{1}{16\pi(s-4m_\pi^2)}\int_{4m_\pi^2-s}^{0} {\rm d}t\mathcal{A}^{\rm LO}(t). \tag{23}$$

Function $I_{tu}(s)$ in Eq. (21) comes from the partial wave projection of the crossed t- and u-channel amplitudes. The bound state in the crossed channels also generates a left-hand cut with a branch point at $4m_\pi^2 - m_\sigma^2$. However, this amplitude does not satisfy the exact unitarity any more. Thus, to partially recover crossing symmetry and restore unitarity, we need to resort to some unitarization methods, e.g. the inverse amplitude method (IAM, see Ref. [61] and references therein) and the N/D method [62]. The situation here is not suitable for direct application of IAM, because the partial wave amplitude Eq. (21) is not a complete calculation at $\mathcal{O}(1/N)$ and thus will break even the perturbative version of the unitarity relation, namely

$$\begin{aligned}{\rm Im}\mathcal{T}_{00}^{\rm NLO} &= \rho\left[\mathcal{T}_{00}^{\rm LO}(\mathcal{T}_{00}^{\rm NLO})^* + (\mathcal{T}_{00}^{\rm LO})^*\mathcal{T}_{00}^{\rm NLO}\right] \\ &= \frac{2\rho{\rm Re}\mathcal{T}_{00}^{\rm LO}{\rm Re}\mathcal{T}_{00}^{\rm NLO}}{1 - 2\rho{\rm Im}\mathcal{T}_{00}^{\rm LO}},\end{aligned} \tag{24}$$

where we also represent ${\rm Im}\mathcal{T}_{00}^{\rm NLO}$, i.e. the imaginary part of the next-to-leading order amplitude, in terms of ${\rm Im}\mathcal{T}_{00}^{\rm LO}$ and ${\rm Re}\mathcal{T}_{00}^{\rm NLO}$ after simple algebraic calculations. Nevertheless, it is still possible to acquire an approximation of the

$\mathcal{O}(1/N)$ partial wave (denoted by $T_{00}^{\mathrm{NLO}\prime}$) that does satisfy the above relation by setting $\mathrm{Re}\mathcal{T}_{00}^{\mathrm{NLO}} = -\frac{1}{N}\mathrm{Re}\mathcal{T}_{00}^{\mathrm{LO}} + I_{tu}$ and obtaining $\mathrm{Im}\mathcal{T}_{00}^{\mathrm{NLO}}$ using Eq. (24). After the analytic continuation of the modified amplitude $T_{00}^{\mathrm{NLO}\prime}$, the approximated "IAM unitarized amplitude" $\mathcal{T}_{00}^{\mathrm{IAM}}$ can be constructed as usual:

$$\mathcal{T}_{00}^{\mathrm{IAM}} = \frac{(\mathcal{T}_{00}^{\mathrm{LO}})^2}{\mathcal{T}_{00}^{\mathrm{LO}} - \mathcal{T}_{00}^{\mathrm{NLO}\prime}}. \tag{25}$$

However, this unitarized amplitude is found to have spurious poles both on the first and second sheets that may not be simply removed. Thus in the following we will use the N/D method.

III. σ POLE IN N/D MODIFIED $O(N)$ MODEL WITH VARYING m_π

It has been seen that in the $O(N)$ model the isospin projection to the $I = 0$ channel breaks crossing symmetry at the leading order of $1/N$ expansion. The $O(N)$ amplitude must be modified in order to at least partially recover crossing symmetry while preserving unitarity. The key point is to generate the left-hand cut from crossed channels in the scattering amplitude, which should be consistent with the bound state the σ generated. It is well known that the N/D method can introduce the left-hand cut contribution to the amplitude and at the same time preserve partial wave unitarity, which is suitable for the purposes here.

In the spirit of the N/D method, the $\mathcal{T}$ matrix can be expressed as

$$\mathcal{T}(s) = \frac{N(s)}{D(s)}, \tag{26}$$

where the singularity of $N(s)$ contains only the left-hand cut (L), while $D(s)$ only contains the right-hand cut (R) and Castillejo-Dalitz-Dyson (CDD) poles [63], thus $\mathrm{Im}_R N(s) = \mathrm{Im}_L D(s) = 0$. To satisfy the partial wave unitarity relation, i.e. $\mathrm{Im}_R \mathcal{T}^{-1} = -\rho$, the relation between $N(s)$ and $D(s)$ should be

$$\mathrm{Im}_R D(s) = -\rho(s) N(s), \tag{27}$$

$$\mathrm{Im}_L N(s) = D(s)\mathrm{Im}_L T(s). \tag{28}$$

Using the Cauchy integral formula, one can write down dispersion relations for $N(s)$ and $D(s)$, and then solve $N(s)$ and $D(s)$ numerically to obtain the scattering amplitude.

Our strategy is to extract the $\mathrm{Im}_L\mathcal{T}$ from the $O(N)$ model, use the N/D method to obtain the scattering amplitude, which at the leading $1/N$ order recovers the original $O(N)$ model amplitude, and require the position of the σ bound state to be consistent with the left-hand cut branch point at $s_L = 4m_\pi^2 - m_\sigma^2$ for large unphysical m_π. Since the numerator and denominator of the amplitude in Eq. (18) both have an s power less than s^2 as $s \to \infty$, it is natural to use *twice subtracted* dispersion relations for $N(s)$ and $D(s)$ without CDD poles, and as a bonus, the zero point of the $\mathcal{T}$ matrix can be dynamically generated, which could correspond to the Adler zero. The twice subtracted dispersion relations for $N(s)$ and $D(s)$ can be expressed as

$$D(s) = \frac{s - s_A}{s_0 - s_A} + g_D \frac{s - s_0}{s_A - s_0} - \frac{(s - s_0)(s - s_A)}{\pi} \times \int_R \frac{\rho(s')N(s')}{(s' - s)(s' - s_0)(s' - s_A)} \mathrm{d}s', \tag{29}$$

$$N(s) = b_0 \frac{s - s_A}{s_0 - s_A} + g_N \frac{s - s_0}{s_A - s_0} + \frac{(s - s_0)(s - s_A)}{\pi} \times \int_L \frac{D(s')\mathrm{Im}_L\mathcal{T}(s')}{(s' - s)(s' - s_0)(s' - s_A)} \mathrm{d}s', \tag{30}$$

where the subtraction points $s_A = m_\pi^2$, $s_0 = s_{th} = 4m_\pi^2$, and $D(s_0) = 1$ are chosen for convenience. With these choices, the subtraction constants are $N(s_0) = b_0$, $N(s_A) = g_N$, $D(s_A) = g_D$. Noticing that at $s_A = m_\pi^2$, the leading order partial wave amplitude in Eq. (18) is zero, corresponding to the leading order Adler zero. Then with $\mathcal{T}(s_A) = N(s_A)/D(s_A) \sim \mathcal{O}(1/N)$, one can choose g_N to be $\mathcal{O}(1/N)$ and g_D to be $\mathcal{O}(1)$. Thus to the leading order, $N(s) = b_0 \frac{s - s_A}{s_0 - s_A}$. By substituting this into Eq. (29) one recovers the leading order scattering amplitude by choosing

$$b_0 = -\frac{1}{32\pi} \frac{s_0 - s_A}{(s_0 - s_A)B(s_0, m_\pi, M) - f_\pi^2/N}, \tag{31}$$

$$g_D = \frac{32\pi f_\pi^2 b_0}{N(s_0 - s_A)}. \tag{32}$$

It is obvious that b_0 is just the leading order amplitude which is consistent with our prescription $N(s_0) = b_0$ and $D(s_0) = 1$. After including t- and u-channel contributions in the N/D construction, the amplitude recovers unitarity and has a left-hand cut with a branch point at $4m_\pi^2 - m_\sigma^2$ when $m_\pi > m_c$, which is as expected. However, since the σ pole in the crossed channels is still located at the same position in the leading order amplitude, the branch point at $4m_\pi^2 - m_\sigma^2$ is determined by the leading order m_σ in $1/N$ expansion. But with the $\mathcal{O}(1/N)$ left-hand cut contribution in $D(s)$, the mass of the σ bound state may be shifted from the pole position of $\mathcal{T}_{00}^{\mathrm{LO}}$. To be consistent with the left-hand cut, demanded by crossing symmetry, we need to require the σ bound state pole position [solved from $D(s) = 0$] to be the same as the one in leading order amplitude. In general, this can be achieved by properly choosing the higher order corrections to the parameters b_0

and g_D. For $m_\pi > m_c$ this can only be done numerically, our prescription is as follows:

$$b_0 = \mathcal{T}_{00}(s_0) = \frac{N-1}{32\pi}\mathcal{A}^{\mathrm{LO}}(s_0) + I_{tu}(s_0), \tag{33}$$

$$D(m_\sigma^2) = 0, \tag{34}$$

$$\frac{g_N}{g_D} = \mathrm{Re}I_{tu}(s_A). \tag{35}$$

where b_0 is chosen as the amplitude evaluated at s_0 with the crossed channels added, g_D is determined by requiring the bound state pole position to be the same as the leading order result $s_\sigma = m_\sigma^2$, and Eq. (35) results directly from the requirement $\mathcal{T}(s_A) = \mathcal{T}_{00}(s_A)$ while $s_L < s_A$ [64]. When $m_\pi < m_c$, Eq. (34) is replaced by Eq. (32) with Eqs. (33) and (35) not changed. This prescription for the subtraction constants captures the most important features of the inputted $O(N)$ model. Anyway, it is of course not the "unique solution" for N/D modified $O(N)$ model. We also tried several different sets of subtraction constants, and found that the qualitative results for the σ pole trajectory are quite robust.

The numerical results of the pole structure as m_π increases are shown in Fig. 2. In order to obtain a σ pole close to the one in the leading order $O(N)$ amplitude at physical pion mass, the intrinsic scale M is set to 1.5 GeV with $m_c \simeq 214$ MeV accordingly. When pion mass increases from the physical value $m_\pi = 139$ MeV, the σ poles move towards the real axis and at some point they hit the real axis and separate into two virtual state poles, with one moving up (VS I) and the other moving down (VS II) along the real axis. The upper virtual state, VS I, moves across the threshold to the physical Riemann sheet and then moves down along the real axis, hence becoming a bound state. At the same time, there will be a left-hand cut generated with the branch point located at $s_L = 4m_\pi^2 - m_\sigma^2 > 0$ in the partial wave amplitude, which comes from the σ exchange in the t- and u-channels from crossing symmetry. During this course but before VS I turns into a bound state, an additional virtual state pole (VS III) is generated from the left-hand cut, which was also implied in Ref. [58]. With m_π growing larger, VS II and VS III hit each other, move into the complex plane, and become a pair of subthreshold poles. In fact, in Ref. [57], it was shown that besides a σ bound state below the threshold, there is also a pair of conjugate poles below the threshold when $m_\pi = 391$ MeV, which corresponds to the pair of subthreshold poles in Fig. 2. It was argued that such subthreshold poles are inevitable due to the behavior of the left-hand cut generated from the σ exchange in crossed t- and u-channels.

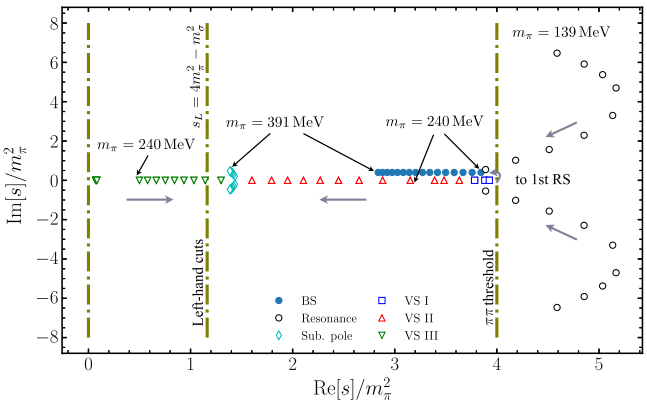

FIG. 2. The pole trajectories for the N/D modified $O(N)$ model. The left-hand cut branch point extends to $s_L = 4m_\pi^2 - m_\sigma^2$ after the virtual state pole VS I moves across threshold to the physical Riemann sheet, turning into a bound state. Qualitatively, the N/D modified $O(N)$ model reproduces the picture derived from K-matrix [49,51] and Roy-equation [57,58] analyses of the lattice data.

A more careful argument goes as follows. Considering that the S matrix near s_L is mainly contributed by the singular behavior of the branch point of the log cut generated from the cross-channel σ bound state pole, if the residue of the σ pole is positive [65], which is always the case in practice, the sign of the partial wave S-matrix immediately above s_L on the real axis can be proved to be negative (opposite to the sign of the residue). If m_π is not large enough such that VS II is still on the real axis, the S matrix below threshold between s_L and the σ pole should have two zero points as shown in the middle graph of Fig. 3. The two zeros of S matrix mean that besides VS II generated from the original σ poles another virtual state pole VS III is generated from the branch point of the left-hand cut [67]. As the pion mass increases further, the S matrix between the branch point and the bound state becomes smaller such that VS II and VS III move toward each other, and then they hit each other at some point and move into the complex plane, becoming a new resonance. The final situation is illustrated in the right graph of Fig. 3 and is what is found at $m_\pi = 391$ MeV. Admittedly, both the above argument and the one in Ref. [57] can only ensure the existence of VS III when there is a σ bound state.

However as pointed out above, the situation is a little different in the N/D modified $O(N)$ model, where the additional virtual state pole, VS III, is generated before the σ becomes a bound state (see the left graph of Fig. 3), i.e. without the left-hand cut generated by the σ-bound-state exchange in the crossed channels. The origin of this VS III state is found to be related with the interplay of Adler zero and the left-hand cut. As m_π increases, we found that the real Adler zero, moving toward the left-hand cut, will hit the branch point $s_L = 0$ and go into the complex plane, becoming a pair of conjugate zeros. Remarkably, complex Adler zeros at $m_\pi \sim 391$ MeV were first found in Ref. [57] and real Adler zero cannot be found in Ref. [58] for $m_\pi \sim 283$ MeV, which may indicate that the above behavior of the

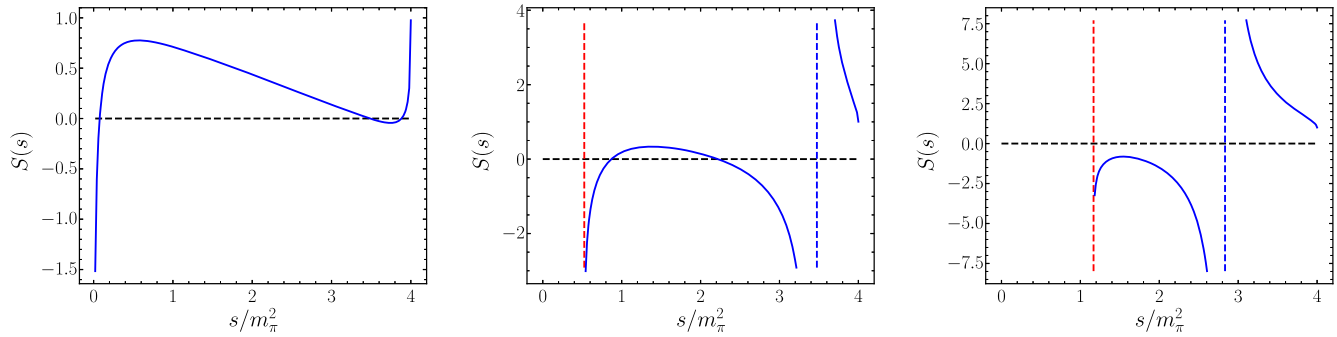

FIG. 3. Blue solid line: physical-sheet S matrix below threshold obtained in the N/D modified $O(N)$ model. Blue dashed line: position of the σ bound state. Red dashed line: branch point of the left-hand cut ($s_L = 4m_\pi^2 - m_\sigma^2$). The left graph ($m_\pi = 207$ MeV): two virtual states in the near threshold region and one additional virtual state pole generated close to the left-hand cut. The middle graph ($m_\pi = 283$ MeV): one bound state with two virtual states. The right graph ($m_\pi = 391$ MeV): two virtual state poles have become a pair of resonance poles.

Adler zero could be general. Then, it is straightforward to prove that VS III is generated when Adler zero passes s_L as follows. The partial wave S matrix is defined as $S(s) = 1 + 2i\rho(s)\mathcal{T}(s)$, thus $S(s) \to -\text{sign}(\mathcal{T}(s))\infty$ when $s \to s_L + 0^+$, as long as $\lim_{s\to s_L+0^+} \mathcal{T}(s) \neq 0$. [68] Then the Adler zero, i.e. the simple zero point of $\mathcal{T}(s)$, passing s_L, causes a sign change of $\mathcal{T}(s)$ from negative to positive and hence also a sign change of $S(s)$, at $s \to s_L + 0^+$. This phenomenon has to occur before the σ turns into a bound state, since according to the argument of the previous paragraph, the sign of S matrix close to the branch point cannot be flipped when σ remains a bound state. Considering that the S matrix equals to 1 both at the threshold and at the Adler zero, there can only be even number of S-matrix zeros between these two points. Thus before the Adler zero passes s_L, if there are two virtual states, i.e. VS I and II, generated after the σ resonance poles hit the real axis, they must both be within that region. For smaller m_π values, if there is no VS III and the Adler zero has not hit the left-hand cut branch point yet, thus $S(s)$ is zero-free between the Adler zero and s_L. Then $S(s)$ has to be positive on that interval. When Adler zero moves through the branch point, it causes the sign of S matrix near the left-hand cut changing from positive to negative. This sign flip of $S(s)$ in the vicinity of s_L indicates the generation of a S-matrix zero point from the branch point of the left-hand cut as shown in the left graph in Fig. 3, which exactly results in the appearance of VS III. As the pion mass grows further, the situation is similar to the description in the previous paragraph where VS I moves to the first sheet becoming a bound state, and VS II hit VS III then both moving into the complex plane. Thus, the existence of VS III and hence the subthreshold poles at large pion mass, e.g. $m_\pi \sim 391$ MeV, is actually the combined result of unitarity, crossing symmetry, Adler zero (which is a significant feature for low energy chiral dynamics) and the analyticity of the S matrix in this region.

The N/D modified $O(N)$ model reproduces the picture derived from Roy-equation analyses, which demonstrates that the σ particle in the $O(N)$ model really can represent, *at the qualitative level*, the f_0 state extracted by Roy equation from the lattice data. Conversely, this also means that the lowest f_0 state in the low energy $\pi\pi$ scattering really plays the similar role of the σ in $O(N)$ linear σ model—providing the vacuum expectation value for spontaneous breaking of chiral symmetry.

IV. σ POLE TRAJECTORY WITH TEMPERATURE FOR DIFFERENT m_π

It is also instructive to look at the σ pole trajectory in a finite temperature environment. It is well known that in the chiral limit, i.e., when the pion is massless at zero temperature, under high temperature the system goes through a phase transition from the chiral symmetry broken phase to the chiral symmetric phase at a critical temperature T_c [69–72] (e.g. for $O(N)$ model without explicit symmetry breaking [73,74], $T_c = \sqrt{12/N} f_\pi \simeq 160$ MeV, which can be easily read out in Fig. 4). One would expect that above the phase transition temperature the massless pion gets massive and the σ particle would be degenerate with pions. With explicit chiral symmetry breaking where the pion has a mass at zero temperature, there is no explicit phase transition point. But with temperature going higher and higher, the system asymptotically approaches the chiral symmetric phase, where the mass of the sigma tends to the pion mass. Notice that this whole picture cannot be explicitly realized in χPT, since it is constructed intrinsically in the broken phase. This means that χPT is valid only for an energy or temperature far below the chiral symmetry breaking scale, which is determined by the VEV of the scalar field or $\bar{q}q$. Under each of the circumstances, (a) the VEV approaches zero, or (b) the energy scale or (c) the temperature becomes comparable with or goes

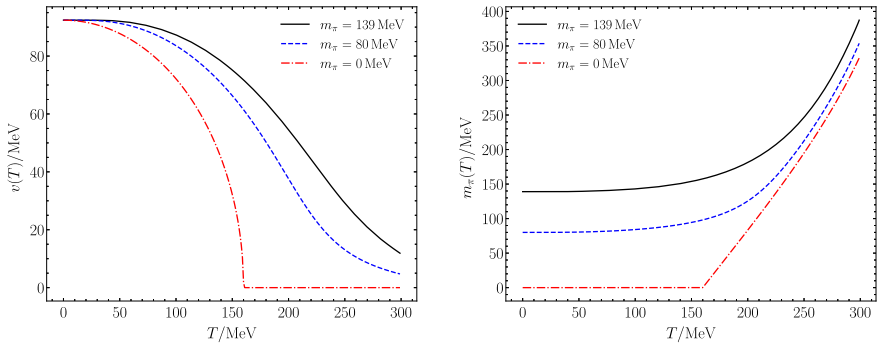

FIG. 4. $v(T)$ (left) and $m_\pi(T)$ (right). The three cases are identified by $m_\pi(0) = 139$, 80, and 0 MeV. In the chiral limit, there is a second-order phase transition with the critical temperature $T_c \simeq 160$ MeV. With a nonzero $m_\pi(0)$, there is no explicit transition point.

beyond the chiral symmetry breaking scale, the whole theory breaks down. For example, in Refs. [34,36], the σ pole was found to be still in the complex plane of the second Riemann sheet around $T = 200$ MeV, which seems to be hopeless to restore the $O(4)$ symmetry in χPT around T_c.

The above picture can be easily seen in the $O(N)$ linear σ model. The leading order effective potential at finite temperature T can be obtained with imaginary-time formalism [73–76] by Wick rotation to Euclidean space and substituting the momentum integral with a sum over Matsubara frequencies $\omega_n = 2\pi nT$, i.e. $\int \frac{d^4k}{(2\pi)^4} f(k_0, \mathbf{k}) \to iT \sum_n \int \frac{d^3\mathbf{k}}{(2\pi)^3} f(k_0 = i\omega_n, \mathbf{k})$ (see, e.g. Ref. [77] for details). The renormalization condition is chosen the same as the $T = 0$ case. Then by minimizing the effective potential, we can obtain the gap equations for v and m_π^2 as functions of temperature [74]:

$$v^2(T) = f_\pi^2 + \frac{N}{16\pi^2}\left(m_\pi^2 \log\frac{m_\pi^2}{M^2} - m_\pi^2(T)\log\frac{m_\pi^2(T)}{M^2}\right) - NA^{T\neq 0}\big(m_\pi^2(T)\big), \tag{36}$$

$$\alpha = v(T)m_\pi^2(T), \tag{37}$$

where $v(0) = f_\pi$ and $m_\pi(0) = m_\pi$ are set to zero-temperature values. The function $A^{T\neq 0}$ is defined as the finite temperature contribution to the tadpole integral encountered in the derivation of Eq. (7),

$$A^{T\neq 0}(m_\pi^2(T)) = \int_0^\infty \frac{dk}{2\pi^2}\frac{k^2 n_B(\omega_k)}{\omega_k}, \tag{38}$$

where $\beta = 1/T$, $\omega_k = \sqrt{k^2 + m_\pi^2(T)}$ and $n_B(\omega_k) = (e^{\beta\omega_k} - 1)^{-1}$ is the Bose-Einstein distribution. With different values of $m_\pi(0)$, denoting the magnitude of explicit breaking, the solutions of $v(T)$ and $m_\pi(T)$ are shown in Fig. 4.

To study the spectrum at finite temperature in the center-of-mass (CM) frame, the scattering amplitude is generalized to be the amputated four-point Green's function with the external momenta analytically continued back to on-shell momenta in Minkowski space after the Matsubara sum [36,78–80]. The leading $1/N$ order $\pi\pi$ scattering amplitude with finite temperature can be expressed as

$$\mathcal{T}_{00}^T(s) = -\frac{1}{32\pi}\frac{s - m_\pi^2(T)}{(s - m_\pi^2(T))B^T(s, m_\pi(T), M) - v^2(T)/N}, \tag{39}$$

where $B^T(s, m_\pi(T), M)$, the finite temperature version of $B(s, m_\pi, M)$ defined in Eq. (14), can be obtained by standard calculations,

$$B^T(s, m_\pi(T), M) = B(s, m_\pi(T), M) + B^{T\neq 0}(s, m_\pi(T)), \tag{40}$$

$$B^{T\neq 0}(s, m_\pi(T)) = \int_0^\infty \frac{dk k^2}{8\pi^2\omega_k^2} n_B(\omega_k) \times \left(\frac{1}{E + 2\omega_k} - \frac{1}{E - 2\omega_k}\right), \tag{41}$$

with $B^{T\neq 0}$ evaluated in the CM frame and $s = E^2$. The σ resonance pole can be obtained from the zero point of the denominator of $\mathcal{T}_{00}^T$ on the second Riemann sheet. The mass and width for the σ pole with varying temperature and with $m_\pi(0) = 200$, 139, and 80 MeV respectively are illustrated in Fig. 5, in which m_σ and Γ_σ are also compared to the behavior of m_π at finite temperature for each case. As temperature increases, σ resonance firstly becomes even broader due to the growth in phase space caused by the Bose-Einstein distribution $n_B(\omega_k)$, and then Γ_σ drops rapidly to zero when σ turns into a pair of virtual state poles. For the present purpose, to demonstrate the asymptotic degeneration of σ and π's, we only keep track of the virtual state pole, VS I (named in the same way as the zero-temperature case), which moves up through threshold to the physical sheet and becomes a σ bound state at around T_c. Then m_σ changes gradually and moves closer to $m_\pi(T)$ when $T > T_c$. Furthermore, m_σ and $m_\pi(T)$ asymptotically

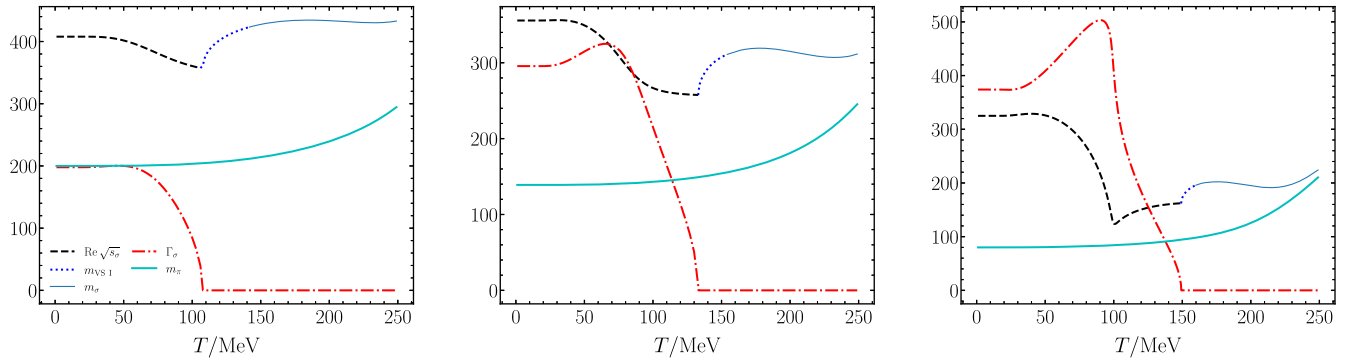

FIG. 5. The mass and width of σ pole with varying temperature compared with $m_\pi(T)$. From left to right, $m_\pi(0) = 200$, 139, and 80 MeV respectively. The lower virtual state pole VS II is not shown above.

tends to converge at $T \gg T_c$, which is as expected by the restoration of chiral symmetry at high temperature limit.

V. CONCLUSIONS AND DISCUSSIONS

In this paper, we have investigated the $O(N)$ linear σ model with varying m_π to reproduce the subthreshold pole structure of the $IJ = 00$ channel $\pi\pi$ scattering amplitude, recently found using the Roy equation in analyzing the lattice phase shifts at several unphysical m_π values. By using the N/D method to partially recover crossing symmetry of the partial wave amplitude in the $O(N)$ model, the Roy-equation analysis results can be roughly reproduced. The pole trajectory illustrates the picture that with large m_π, as the Adler zero goes into the complex plane before σ becomes a bound state, besides the virtual state accompanying the σ bound state, another virtual state pole will originate from the left-hand cut. As m_π grows larger, the two virtual state poles hit each other and scatter into the complex plane and become a pair of resonance poles.

The consistency of the $O(N)$ model with the Roy-equation analyses reveals that the lowest f_0 state from the Roy-equation analyses of the lattice data can be fairly described by the σ field in the $O(N)$ linear σ model, thus plays the same role in the chiral symmetry breaking as the σ particle in $O(N)$ model.

The σ pole behavior with varying temperature is also discussed in the $O(N)$ model with different pion masses. It is shown that with higher temperature the sigma resonance pole also moves to the real axis and becomes a pair of virtual states. Then the upper one moves across threshold to the first Riemann sheet and turns into a bound state. With much higher temperatures, the mass of the σ and pion would tend to come closer and closer, which is as expected by chiral symmetry restoration in the high temperature limit.

It is worth mentioning that the $O(N)$ model itself suffers from the vacuum stability problem. In short, the original $O(N)$ model effective potential is obtained by solving the auxiliary field $\chi(\phi^2)$ as a function of ϕ_a from one of the gap equations $\frac{\partial V}{\partial \chi} = 0$, which has two branches of solutions: one with ordinary chiral symmetry breaking vacuum (i.e. $m_\pi \to 0$ when $\alpha \to 0$), the other with a larger pion mass which restores chiral symmetry ($v = 0$ but $m_\pi \neq 0$) in the $\alpha \to 0$ limit [39,81–85]. In perturbation theory, $V(\phi)$ is expanded around the vacuum which is a stationary point of the effective potential. Whether it is a local minimum, local maximum, or saddle point can be determined by the Hessian matrix of $V(\phi)$. After a careful investigation we found that the vacuum chosen at $v = f_\pi$ with $\chi(v^2) = m_\pi^2$ remains a local minimum on the first branch when $m_\pi < M/\sqrt{e}$. However for larger pion mass, the stable minimum exists only on the second branch. This is a warning that when m_π gets large, the vacuum of the $O(N)$ model becomes unstable—a phenomenon not known in our knowledge of QCD [86]. A similar problem also happens at high temperature: when $T \gg T_c$, the effective potential no longer provides a local minimum on its first branch. Instead, the local minimum will move to the second branch and become a saddle point. In spite of these deficiencies, we insist on the opinion that the linear σ model on the first branch provides the correct picture for describing low energy QCD, since high dimensional terms and other resonance terms, missed in the present discussion based on the toy linear sigma model may alleviate the vacuum stability problem. After all, it is worthwhile to look at the m_π dependence of the effective potential which is not discussed in the literature yet, to the best of our knowledge. We will present the details of these discussions elsewhere.

Another direction to be explored is to look at the behavior of the $N^*(920)$ recently found in the πN scattering from the Roy-equation analysis [87–89] under different pion masses or temperatures. The role $N^*(920)$ plays in the πN scattering is in some sense similar to the σ particle in $\pi\pi$ scattering. If it shares similar properties at higher temperatures, one would expect that $N^*(920)$ would become a bound state and the parity partner of the nucleon, and thus may play an important role in physics.

ACKNOWLEDGMENTS

This work is supported by China National Natural Science Foundation under Contracts No. 12335002, No. 12375078, and No. 11975028. This work is also supported by "the Fundamental Research Funds for the Central Universities."

[1] M. Gell-Mann and M. Lévy, Nuovo Cimento **16**, 705 (1960).
[2] M. M. Islam and R. Pinon, Phys. Rev. Lett. **12**, 310 (1964).
[3] S. H. Patil, Phys. Rev. Lett. **13**, 261 (1964).
[4] V. Hagopian, W. Selove, J. Alitti, and J. P. Baton, Phys. Rev. **145**, 1128 (1966).
[5] S. R. Coleman, J. Wess, and B. Zumino, Phys. Rev. **177**, 2239 (1969).
[6] C. G. Callan, Jr., S. R. Coleman, J. Wess, and B. Zumino, Phys. Rev. **177**, 2247 (1969).
[7] J. Gasser and H. Leutwyler, Ann. Phys. (N.Y.) **158**, 142 (1984).
[8] J. Gasser and H. Leutwyler, Nucl. Phys. **B250**, 465 (1985).
[9] G. Ecker, J. Gasser, A. Pich, and E. de Rafael, Nucl. Phys. **B321**, 311 (1989).
[10] J. F. Donoghue, C. Ramirez, and G. Valencia, Phys. Rev. D **39**, 1947 (1989).
[11] Z. H. Guo, J. J. Sanz Cillero, and H. Q. Zheng, J. High Energy Phys. 06 (2007) 030.
[12] Z. H. Guo, J. J. Sanz-Cillero, and H. Q. Zheng, Phys. Lett. B **661**, 342 (2008).
[13] J. R. Pelaez, Mod. Phys. Lett. A **19**, 2879 (2004).
[14] A. Gomez Nicola and J. R. Pelaez, Phys. Rev. D **65**, 054009 (2002).
[15] G.-Y. Qin, W. Z. Deng, Z. Xiao, and H. Q. Zheng, Phys. Lett. B **542**, 89 (2002).
[16] D.-L. Yao, L.-Y. Dai, H.-Q. Zheng, and Z.-Y. Zhou, Rep. Prog. Phys. **84**, 076201 (2021).
[17] Z. Xiao and H. Q. Zheng, Nucl. Phys. **A695**, 273 (2001).
[18] H. Q. Zheng, Z. Y. Zhou, G. Y. Qin, Z. Xiao, J. J. Wang, and N. Wu, Nucl. Phys. **A733**, 235 (2004).
[19] Z. Y. Zhou, G. Y. Qin, P. Zhang, Z. Xiao, H. Q. Zheng, and N. Wu, J. High Energy Phys. 02 (2005) 043.
[20] H. Q. Zheng, Z. Y. Zhou, G. Y. Qin, and Z. Xiao, AIP Conf. Proc. **717**, 322 (2004).
[21] J.-j. Wang, Z. Y. Zhou, and H. Q. Zheng, J. High Energy Phys. 12 (2005) 019.
[22] Z. Y. Zhou and H. Q. Zheng, Nucl. Phys. **A775**, 212 (2006).
[23] S. M. Roy, Phys. Lett. B **36**, 353 (1971).
[24] G. Colangelo, J. Gasser, and H. Leutwyler, Nucl. Phys. **B603**, 125 (2001).
[25] B. Ananthanarayan, G. Colangelo, J. Gasser, and H. Leutwyler, Phys. Rep. **353**, 207 (2001).
[26] I. Caprini, G. Colangelo, and H. Leutwyler, Phys. Rev. Lett. **96**, 132001 (2006).
[27] R. Garcia-Martin, R. Kaminski, J. R. Pelaez, J. Ruiz de Elvira, and F. J. Yndurain, Phys. Rev. D **83**, 074004 (2011).
[28] G. Mennessier, S. Narison, and W. Ochs, Phys. Lett. B **665**, 205 (2008).
[29] G. Mennessier, S. Narison, and X. G. Wang, Phys. Lett. B **688**, 59 (2010).
[30] Z. X. Sun, L. Y. Xiao, Z. Xiao, and H. Q. Zheng, Mod. Phys. Lett. A **22**, 711 (2007).
[31] S. Weinberg, Phys. Rev. Lett. **110**, 261601 (2013).
[32] J. Gasser and H. Leutwyler, Phys. Lett. B **188**, 477 (1987).
[33] P. Gerber and H. Leutwyler, Nucl. Phys. **B321**, 387 (1989).
[34] S. Cortés, A. Gómez Nicola, and J. Morales, Phys. Rev. D **93**, 036001 (2016).
[35] A. Gomez Nicola and J. Ruiz de Elvira, Phys. Rev. D **97**, 074016 (2018).
[36] R. Gao, Z.-H. Guo, and J.-Y. Pang, Phys. Rev. D **100**, 114028 (2019).
[37] L. Dolan and R. Jackiw, Phys. Rev. D **9**, 3320 (1974).
[38] H. J. Schnitzer, Phys. Rev. D **10**, 1800 (1974).
[39] S. R. Coleman, R. Jackiw, and H. D. Politzer, Phys. Rev. D **10**, 2491 (1974).
[40] Z.-H. Guo, L. Y. Xiao, and H. Q. Zheng, Int. J. Mod. Phys. A **22**, 4603 (2007).
[41] M. Luscher, Commun. Math. Phys. **105**, 153 (1986).
[42] M. Luscher and U. Wolff, Nucl. Phys. **B339**, 222 (1990).
[43] M. Luscher, Nucl. Phys. **B354**, 531 (1991).
[44] Y. Kuramashi, M. Fukugita, H. Mino, M. Okawa, and A. Ukawa, Phys. Rev. Lett. **71**, 2387 (1993).
[45] S. He, X. Feng, and C. Liu, J. High Energy Phys. 07 (2005) 011.
[46] N. Mathur, A. Alexandru, Y. Chen, S. J. Dong, T. Draper, I. Horvath, F. X. Lee, K. F. Liu, S. Tamhankar, and J. B. Zhang, Phys. Rev. D **76**, 114505 (2007).
[47] X. Feng, K. Jansen, and D. B. Renner, Phys. Lett. B **684**, 268 (2010).
[48] Z. Fu, Phys. Rev. D **85**, 014506 (2012).
[49] R. A. Briceno, J. J. Dudek, R. G. Edwards, and D. J. Wilson, Phys. Rev. Lett. **118**, 022002 (2017).
[50] H.-W. Lin *et al.* (Hadron Spectrum Collaboration), Phys. Rev. D **79**, 034502 (2009).
[51] A. Rodas, J. J. Dudek, and R. G. Edwards (Hadron Spectrum Collaboration), Phys. Rev. D **108**, 034513 (2023).
[52] C. Hanhart, J. R. Pelaez, and G. Rios, Phys. Rev. Lett. **100**, 152001 (2008).
[53] J. R. Pelaez and G. Rios, Phys. Rev. D **82**, 114002 (2010).
[54] C. Hanhart, J. R. Pelaez, and G. Rios, Phys. Lett. B **739**, 375 (2014).
[55] X.-L. Gao, Z.-H. Guo, Z. Xiao, and Z.-Y. Zhou, Phys. Rev. D **105**, 094002 (2022).
[56] X.-L. Gao, Z.-H. Guo, Z. Xiao, and Z.-Y. Zhou, Phys. Rev. D **107**, 058502 (2023).
[57] X.-H. Cao, Q.-Z. Li, Z.-H. Guo, and H.-Q. Zheng, Phys. Rev. D **108**, 034009 (2023).

[58] A. Rodas, J. J. Dudek, and R. G. Edwards (Hadron Spectrum Collaboration), Phys. Rev. D **109**, 034513 (2024).
[59] R. S. Chivukula and M. Golden, Phys. Lett. B **267**, 233 (1991).
[60] S. L. Adler, Phys. Rev. **137**, B1022 (1965).
[61] A. Gomez Nicola, J. R. Pelaez, and G. Rios, Phys. Rev. D **77**, 056006 (2008).
[62] G. F. Chew and S. Mandelstam, Phys. Rev. **119**, 467 (1960).
[63] L. Castillejo, R. H. Dalitz, and F. J. Dyson, Phys. Rev. **101**, 453 (1956).
[64] If $m_\sigma^2 < 3m_\pi^2$ such that $s_A = m_\pi^2$ is located in the left-hand cut region, then $\mathcal{T}_{00}(s_A)$ is replaced by $\mathrm{Re}\mathcal{T}_{00}(s_A)$.
[65] In the nonrelativistic scattering theory, the residual of the scattering amplitude is related to $-\gamma^2$ for s wave, where $\gamma \in \mathbb{R}$ is defined using the asymptotic behavior of the wave function $\eta(r) \xrightarrow{r\to\infty} \gamma e^{-\alpha r}$ [66], thus the residue for the S matrix at the σ bound state is positive. In relativistic quantum field theory, the positivity of the residue follows from unitarity.
[66] J. R. Taylor, *Scattering Theory: The Quantum Theory of Nonrelativistic Collisions* (John Wiley & Sons, Inc., New York, 1972).
[67] The second sheet S-matrix is the inverse of the one defined on the physical sheet, owing to unitarity and analyticity.
[68] The situation here is similar to but much more complicated than that of physical m_π [19].
[69] R. D. Pisarski and F. Wilczek, Phys. Rev. D **29**, 338 (1984).
[70] A. Bazavov *et al.*, Phys. Rev. D **85**, 054503 (2012).
[71] A. Bazavov *et al.* (HotQCD Collaboration), Phys. Lett. B **795**, 15 (2019).
[72] H. T. Ding *et al.* (HotQCD Collaboration), Phys. Rev. Lett. **123**, 062002 (2019).
[73] A. Bochkarev and J. I. Kapusta, Phys. Rev. D **54**, 4066 (1996).
[74] J. O. Andersen, D. Boer, and H. J. Warringa, Phys. Rev. D **70**, 116007 (2004).
[75] H. Meyers-Ortmanns, H. J. Pirner, and B. J. Schaefer, Phys. Lett. B **311**, 213 (1993).
[76] H. Meyer-Ortmanns, Rev. Mod. Phys. **68**, 473 (1996).
[77] M. L. Bellac, *Thermal Field Theory*, Cambridge Monographs on Mathematical Physics (Cambridge University Press, Cambridge, England, 2011).
[78] E. Quack, P. Zhuang, Y. Kalinovsky, S. P. Klevansky, and J. Hufner, Phys. Lett. B **348**, 1 (1995).
[79] N. Kaiser, Phys. Rev. C **59**, 2945 (1999).
[80] A. Gomez Nicola, F. J. Llanes-Estrada, and J. R. Pelaez, Phys. Lett. B **550**, 55 (2002).
[81] M. Kobayashi and T. Kugo, Prog. Theor. Phys. **54**, 1537 (1975).
[82] L. F. Abbott, J. S. Kang, and H. J. Schnitzer, Phys. Rev. D **13**, 2212 (1976).
[83] A. D. Linde, Nucl. Phys. **B125**, 369 (1977).
[84] W. A. Bardeen and M. Moshe, Phys. Rev. D **28**, 1372 (1983).
[85] W. A. Bardeen and M. Moshe, Phys. Rev. D **34**, 1229 (1986).
[86] The situation of χPT is even worse due to the Oströgradski instability, such that the χPT Hamiltonian is unbounded from below.
[87] X.-H. Cao, Q.-Z. Li, and H.-Q. Zheng, J. High Energy Phys. 12 (2022) 073.
[88] Y.-F. Wang, D.-L. Yao, and H.-Q. Zheng, Eur. Phys. J. C **78**, 543 (2018).
[89] M. Hoferichter, J. R. de Elvira, B. Kubis, and U.-G. Meißner, arXiv:2312.15015.